



A new optical scheme for large-extraction small-aberration vacuum-ultraviolet synchrotron radiation beamlines

Thierry Moreno*

Optics Group, Synchrotron SOLEIL, L'Orme des Merisiers, Saint-Aubin, BP 48, 91192 Gif sur Yvette Cedex, France.

*Correspondence e-mail: thierry.moreno@synchrotron-soleil.fr

Received 15 March 2016

Accepted 20 July 2016

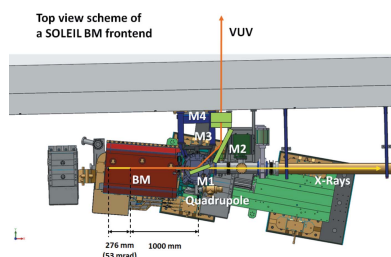
Edited by S. Svensson, Uppsala University, Sweden

Keywords: vacuum-ultraviolet synchrotron beamline; bending magnet; optical aberrations; integration of magnetic and photonic synchrotron beamline components.

Vacuum-ultraviolet radiation delivered by bending-magnet sources is used at numerous synchrotron radiation facilities worldwide. As bending-magnet radiation is inherently much less collimated compared with undulator sources, the generation of high-quality intense bending-magnet vacuum-ultraviolet photon beams is extremely demanding in terms of the optical layout due to the necessary larger collection apertures. In this article, an optimized optical layout which takes into account both the optical and electron beam properties is proposed. This layout delivers an improved beam emittance of over one order of magnitude compared with existing vacuum-ultraviolet bending-magnet beamlines that, up to now, do not take into account electron beam effects. The arrangement is made of two dedicated mirrors, a cylindrical and a cone-shaped one, that focus independently both the horizontal and the vertical emission of a bending-magnet source, respectively, and has been already successfully applied in the construction of the infrared beamline at the Brazilian synchrotron. Using this scheme, two vacuum-ultraviolet beamline designs based on a SOLEIL synchrotron bending-magnet source are proposed and analysed. They would be useful for future upgrades to the DISCO beamline at SOLEIL and could be readily implemented at other synchrotron radiation facilities.

1. Introduction

Vacuum-ultraviolet (VUV) radiation on third-generation synchrotron radiation (SR) sources is increasingly used for structural and functional biology studies based on circular dichroism (CD) spectroscopy (Sutherland *et al.*, 1980; Hoffmann *et al.*, 2007; Réfrégiers *et al.*, 2012). At SR facilities, VUV radiation emitted by bending-magnet (BM) sources is orders of magnitude brighter than conventional VUV sources, providing a higher signal-to-noise ratio in CD experiments over a wide and tunable spectral range. However, because the use of BM sources requires large horizontal apertures in order to increase intensity, significant geometrical aberrations can be introduced by the circular trajectory of the BM source if they are not corrected for. An optical layout, consisting of two optimized shaped mirrors which focus separately the horizontal and the vertical BM emission and remove almost completely the beam aberrations, has been developed in the infrared (IR) domain and successfully applied to the construction of the IR beamline at the Brazilian synchrotron (Moreno *et al.*, 2013). Another method to achieve almost distortion-free focusing of BM sources is to use the well known magic mirror (López-Delgado & Szwarc, 1976). This single mirror design is presently used with very good results at SPring-8 (Kimura *et al.*, 2001) and HASYLAB (Zimmerer, 2007).



© 2016 International Union of Crystallography

In the following, our optimized layout is proposed for two VUV beamline front-ends based on a SOLEIL BM source. The first design (§3.2) uses a common horizontal VUV beamline aperture of 50 mrad, which maintains the current magnetic configuration of a SOLEIL BM front-end and makes the layout easily adaptable to existing VUV BM beamlines. The second design (§3.3) allows for larger horizontal extractions (100 mrad) but requires modifications of the BM and quadrupole chambers by placing the first two mirrors of the beamline close to the BM source. This second example represents an interesting attempt to efficiently integrate magnetic and photonic synchrotron beamline components. Both of these proposals deliver high intensity and almost aberration-free photon beams and should be considered for future upgrades to existing VUV SR facilities.

Contrary to the IR domain, where mirror angles have negligible impact on the reflectivity, VUV radiation requires that the mirrors' maximum grazing angle is limited in order to preserve the beam intensity and the degree of circular polarization. Our two proposals are designed in a similar manner to that of the existing front-end of the VUV DISCO beamline (Giuliani *et al.*, 2009) which includes four silicon mirrors with grazing-incidence angles of 22.5° where two mirrors are reflecting in the horizontal direction and the remaining two in the vertical direction (Figs. 3, 6 and 7). This optical arrangement preserves both beam intensity and the circular degree of polarization.

Although VUV SR is partially coherent in the transverse direction, optical beam properties can be accurately described using a ray-tracing approach (Moreno & Idir, 2001) without reverting to a full wave-propagation calculation (Chubar & Elleaume, 1998). Besides, ray tracing is currently indispensable in order to properly evaluate the geometrical aberrations produced by the circular BM source trajectory and mirror profiles.

2. Method

The proposed optical layout consists of two front-end optics that focus independently the horizontal and vertical emission of the BM source by using cylindrical and cone-shaped mirrors, respectively. The main parameters of these two mirrors, such as their positions inside the front-end, orientations and radii of curvature, are determined in order to minimize beam aberrations generated by the BM source (Moreno, 2015). An optical path method is used (Noda *et al.*, 1974; Howells, 1992) which is summarized below for the horizontal and the vertical directions.

Horizontally, equations (1), (2) and (3) provide the optical parameters of the cylindrical mirror in order to remove defocus, coma and spherical beam aberrations, respectively, which are generated by the circular shape of the BM source trajectory,

$$\frac{1}{p} + \frac{1}{q} = \frac{2}{R \sin(\theta)}, \quad (1)$$

Table 1

Main parameters of the SOLEIL machine and BM source.

Electron energy, current	$E_0 = 2.739 \text{ GeV}, I_0 = 0.5 \text{ A}$
Bending magnet	$B = 1.71 \text{ T}, \rho = 5.28 \text{ m}$
Electron beam size	$\sigma_{eX} \times \sigma_{eZ} = 63.1 \mu\text{m} \times 32.4 \mu\text{m RMS (H} \times \text{V)}$
Electron beam divergence	$\sigma'_{eX} \times \sigma'_{eZ} = 135 \mu\text{rad} \times 2 \mu\text{rad RMS (H} \times \text{V)}$

$$\frac{p}{q} = \left[1 - \frac{2\rho \tan(\theta)}{3p} \right]^{1/2}, \quad (2)$$

$$\frac{p}{q} \left(\frac{3p}{q} - 1 \right)^2 = \tan^2(\theta) \left(1 - \frac{p}{q} \right)^2, \quad (3)$$

where p , q , R and θ are the source and image distances of the cylindrical mirror, its radius of curvature and the grazing angle, respectively, and ρ is the radius of curvature of the BM source.

In the vertical direction, a cone-shaped mirror is used to correct for vertical BM aberrations. Equation (4) gives the local radius of curvature of this mirror as a function of the position x along its axis of symmetry,

$$R(x) = \frac{2pq}{\sin(\theta)(p+q)} \left[1 - \frac{q\rho k}{p^2(p+q)}x + \dots \right], \quad (4)$$

where p , q and θ are the source and image distances of the cone-shaped mirror and its grazing angle, respectively, and ρ is the radius of curvature of the BM source.

The parameter k in equation (4) takes into account the divergence of the beam impinging on the mirror: $k = 1$ if the mirror is placed after the source or $k = M_H/(L_H/p - 1)$ if it is placed after the cylindrical mirror, which is the case for our proposed optical schemes. Here, M_H and L_H are the horizontal magnification and the source-to-image distance of the cylindrical mirror, respectively, and p is the source distance of the cone-shaped mirror. The vertical coma aberration is removed by using equal image and source distances.

This layout has been successfully demonstrated and employed in the IR domain (Moreno *et al.*, 2013) and can be easily transferred to the VUV region. It should be pointed out, however, that the necessity to restrict the mirror grazing angles in the VUV region also reduces somewhat the flexibility of the optical configuration.

3. Application

The method described above is now applied in the design of two proposed VUV beamline front-ends. Calculations are made considering the VUV spectral range 3–20 eV and front-ends consisting of four silicon mirrors with grazing angles of 22.5°. Table 1 provides the main electronic parameters of the SOLEIL machine and BM source.

The photon source size results from the convolution of three components: the electron beam size, the limit of diffraction at the working energy and the geometrical aberrations produced by the circular shape of the source trajectory. The limit of diffraction remains smaller than the electron

beam sizes in the VUV spectral range. Therefore, the best optical configuration is obtained when the geometrical aberrations are kept lower than or of the same order of the electron beam size. It is important to stress that the geometrical aberrations depend on the beamline aperture and the level of aberrations that can be removed by the cylindrical and the cone-shaped mirrors.

3.1. Optimization of the cylindrical mirror

The purpose of the cylindrical mirror is to remove aberrations in the horizontal direction due to BM emission. Fig. 1 shows the horizontal root-mean-square (RMS) size of the spherical aberrations focused by the cylindrical mirror (grazing angle = 22.5°) and back-propagated to the source location as a function of its source distance p for horizontal apertures of 50 mrad and 100 mrad. The radius R and the image distance q of this mirror are defined through equations (1) and (2) in order to remove the horizontal defocus and coma aberrations emitted by the source, respectively. The best mirror configuration that removes defocus, coma and spherical aberrations is obtained for $p = 1.820$ m, $q = 4.080$ m and $R = 6.578$ m, and can be potentially used to extract beams with a very low level of geometric aberrations from horizontal BM apertures up to an extremely large aperture of 400 mrad (see Fig. 2). However, the mirror must be placed quite close to the BM, which implies complicated modifications of the BM and the quadrupole chambers and which consequently limits the horizontal extraction to 100 mrad (see §3.3). Using smaller horizontal apertures, it is possible to move the cylindrical mirror further away from the source, correct for only the first two aberration terms (defocus and coma), and still preserve a

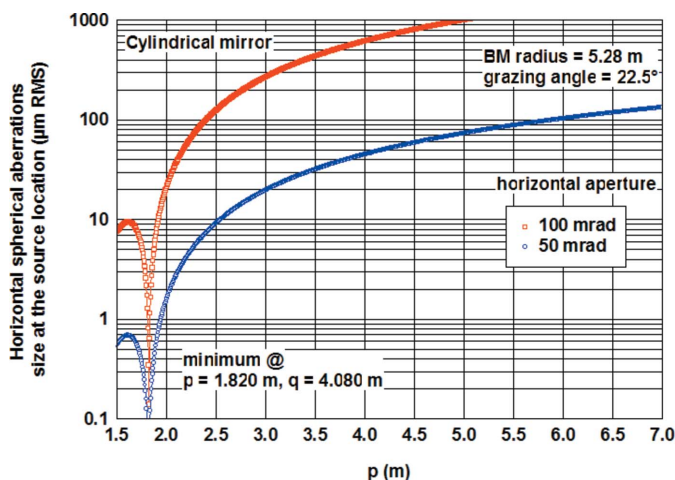


Figure 1 Horizontal RMS size of the spherical aberrations focused by the cylindrical mirror and back-propagated to the source location as a function of the source distance p , for a SOLEIL BM source with horizontal apertures of 50 mrad (blue circles) and 100 mrad (red squares), respectively. The mirror has a grazing angle of 22.5°. The radius R and the image distance q of this mirror are defined through equations (1) and (2) for removing the defocus and coma aberrations, respectively. The minimum at $p = 1.820$ m determines the mirror configuration removing up to and including spherical aberrations and allows for very large horizontal beamline extractions.

high-quality photon beam because the spherical aberration term remains smaller than the electron beam size. Therefore, a good trade-off, which does not modify the BM and quadrupole magnetic chambers and facilitates the upgrade of existing SOLEIL VUV BM beamlines, is to place the cylindrical mirror at 6.3 m from the source by limiting the aperture to 50 mrad (see §3.2). In turn, solving equations (1) and (2) with a fixed grazing angle of 22.5° determines the mirror configuration with $p = 6.3$ m, $q = 7.19$ m and $R = 17.54$ m. Another important point to note is the orientation of the cylindrical mirror curvature with respect to that of the BM source. As the mirror magnification is greater than 1 ($p < q$), both the mirror and the BM curvatures must follow the same orientation (Moreno, 2015).

Fig. 2 shows the back-propagated horizontal beam size at the source location for proposed cylindrical mirrors correcting up to and including for coma or spherical aberrations. For a 50 mrad horizontal aperture ($p = 6.3$ m), defocus and coma aberrations are corrected, while, for the 100 mrad aperture ($p = 1.824$ m), spherical aberration is also cancelled. These calculations are performed both for geometrical BM aberrations alone and also including full source size contributions (electron beam size, geometrical aberrations and the diffraction-limited photon emission at 3 eV). Fig. 2 shows that, for equal beam size and including spherical aberration corrections, a factor of eight can be theoretically gained compared with 50 mrad extraction by placing the cylindrical mirror in close proximity to the BM source and using a horizontal aperture of 400 mrad. For the proposed 100 mrad extraction, a factor of two is gained.

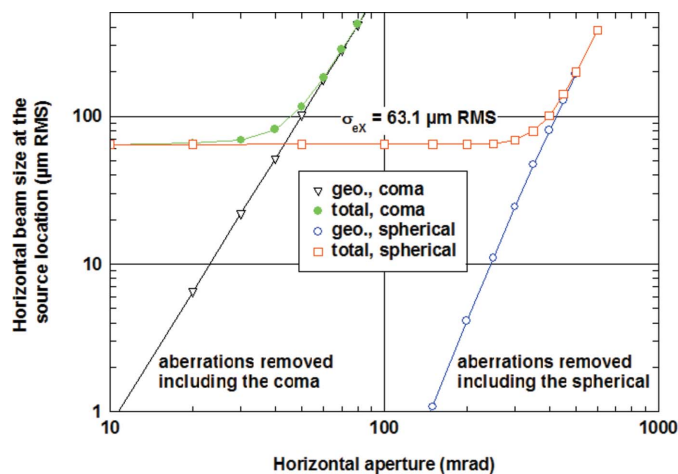


Figure 2 Horizontal RMS beam size focused by the cylindrical mirror and back-propagated to the source location as a function of the horizontal aperture. Calculations are performed considering both the geometrical aberrations alone with the cylindrical mirror removing aberrations including coma, spherical term excluded (black triangles, ‘geo., coma’) and spherical term included (empty blue circles, ‘geo., spherical’). These terms are then added quadratically to the other source size contributions (electron beam, geometrical aberrations and the diffraction-limited photon emission at 3 eV) to give the total horizontal back-propagated source size labeled ‘total, coma’ (green filled circles) and ‘total, spherical’ (empty red squares), respectively.

Table 2

Parameters of the VUV beamline front-end (configuration removing the beam aberrations up to and including coma).

Element	Optical path distance	Geometry	Footprint @ 99%, $E = 3$ eV, length \times width
Diaphragm		50 mrad \times 10 mrad (H \times V)	–
Cold finger	4.975 m	Thickness = 7.5 mm	–
M1 mirror	5.8 m	Plane, $\theta = 22.5^\circ$, sideward	740 mm \times 50 mm
M2 mirror	6.3 m	Cylinder, horizontal focusing, $\theta = 22.5^\circ$, sideward	800 mm \times 55 mm
M3 mirror	6.8 m	Cone shaped, vertical focusing, $\Delta R/R = \pm 1\%$ over ± 150 mm, $\theta = 22.5^\circ$, upward	150 mm \times 285 mm
M4 mirror	7.2 m	Plane, $\theta = 22.5^\circ$, downward	135 mm \times 270 mm
Focal plane	13.49 m	–	–

These mirror configurations are now applied to the design of two VUV beamline front-ends removing the horizontal BM aberrations, including the coma (§3.2) and including the spherical term (§3.3), respectively.

3.2. Configuration removing aberrations up to and including the coma

This configuration, which does not modify the existing BM and quadrupole chambers, is the easiest way to upgrade the present DISCO beamline front-end. From a beamline aperture of 50 mrad \times 10 mrad (H \times V), it delivers a low aberrated and well focused beam of 215 μm \times 90 μm FWHM (H \times V) at the end of the front-end. Fig. 3 and Table 2 detail the main parameters of the VUV beamline front-end in this configuration, where mirror positions are given as optical path distances from the source.

This front-end uses four silicon mirrors with grazing angles of 22.5°. Its two main components are the cylindrical (M2) and the cone-shaped (M3) mirrors which focus the horizontal and the vertical emission of the BM source onto the same plane, respectively. The M2 cylindrical mirror is placed at $p = 6.3$ m from the source with an image distance of $q = 7.19$ m and removes the horizontal defocus and coma BM aberrations. The M1 plane mirror in sideward reflection geometry is necessary to correctly orient the M2 mirror curvature with that of the BM source. The cone-shaped mirror M3 has a magni-

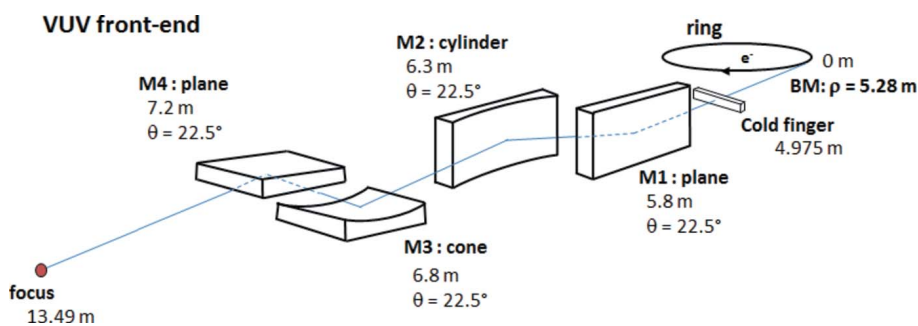


Figure 3

Optical scheme of the SOLEIL VUV beamline front-end with the configuration removing beam aberrations up to and including the coma. Mirror positions are given according to the optical distance from the source.

fication close to 1 ($p = 6.8$ m, $q = 6.69$ m) in order to remove the vertical coma aberrations of the source. With a grazing angle of 22.5° (upward reflection), the best cone-shaped profile $R(x) = R_0(1 + ax)$ is obtained from equation (4) for $R_0 = 17.624$ m and $a = 6.6 \times 10^{-5} \text{ mm}^{-1}$ where x is the coordinate along the axis of curvature of the mirror.

It should be noted that a horizontal cold finger (7.5 mm thickness) is installed in the DISCO front-end, at a distance of 825 mm before the M1 mirror, in order to absorb almost the

entire 3.6 kW emitted by the BM source at 500 mA thus eliminating M1 thermal deformations.

Table 3 provides the optical properties (size, divergence, intensity) of the beam at the exit of the front-end (focal plane) for several VUV energies. Fig. 4 shows the corresponding ray-tracing simulation of the beam image focused at 10 eV, and the Gaussian shape of the focused beam indicates that the beam is almost aberration-free. Fig. 5 compares the vertical angular distributions of intensity (integrated horizontally) and degree of circular polarization of the beam transmitted by the front-end at 10 eV. For CD experiments, the low level of beam aberrations allows to define very precisely vertically areas where the beam is both intense and highly circularly polarized.

It is important to emphasize that, in comparing our proposed layout for a 50 mrad horizontal extraction aperture and correcting for the aberrations generated by the circular trajectory of the BM source, we obtain a significant improvement of over one order of magnitude in the beam emittance (21.7 mm² mrad² at 99% of the encircled energy) compared with the existing DISCO beamline (396 mm² mrad² at 99% of the encircled energy).

3.3. Configuration removing the horizontal aberrations up to and including the spherical term

We consider in this section a possible upgrade of a SOLEIL VUV beamline which requires the modification of the BM and associated quadrupole chambers. Apart from the position of the mirrors and the M1 mirror orientation, this layout is almost identical to the previous one (§3.2). All mirrors are made of silicon with grazing angles of 22.5°. The cylindrical mirror is now placed at $p = 1.82$ m from the source with a focus $q = 4.08$ m. In this configuration, the horizontal aberrations are cancelled up to and including the spherical term and very large horizontal extraction angles are made possible (theoretically up to 400 mrad as shown in Fig. 2). Nevertheless, the horizontal aperture is

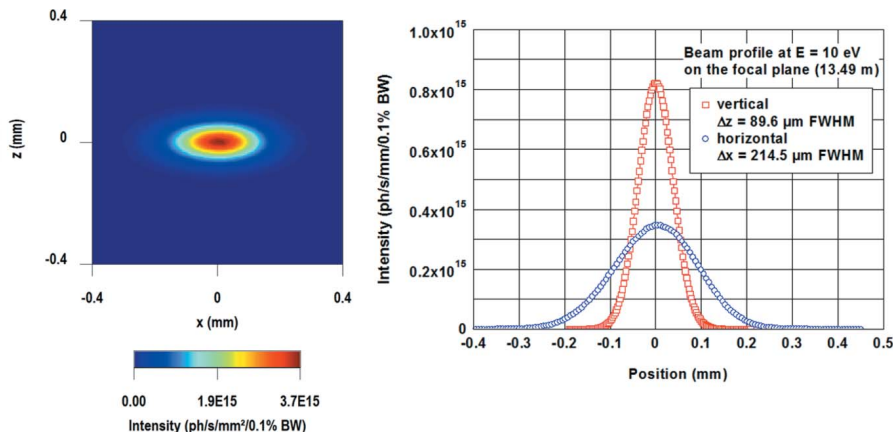


Figure 4 Ray-tracing simulation at 10 eV of the photon beam image (left) and its horizontal and vertical projections (right) focused at 13.49 m from the source in the configuration removing aberrations up to and including the coma. The almost fully Gaussian shape of the focused beam indicates very low level of aberrations.

Table 3

Optical beam properties at the focal plane for three energies in the configuration removing aberrations up to and including the coma.

E (eV)	FWHM size (H × V) (μm)	Divergence (H × V) (mrad @ 99%)	Flux [photons s ⁻¹ (0.1% BW) ⁻¹]
5	215.2 × 92.1	42.7 × 7.0	3.0 × 10 ¹³
10	214.5 × 89.6	42.7 × 5.6	7.8 × 10 ¹³
20	213.9 × 89.0	42.7 × 4.5	1.0 × 10 ¹⁴

limited because of the length of the BM source and space limitations. As in §3.2, a first plane mirror must be placed between the source and the cylindrical mirror in order to preserve the mutual orientation of the source and cylindrical mirror curvatures. This plane mirror has a horizontal slot with an inside triangular aperture varying from 1.2 to 1.7 mm over

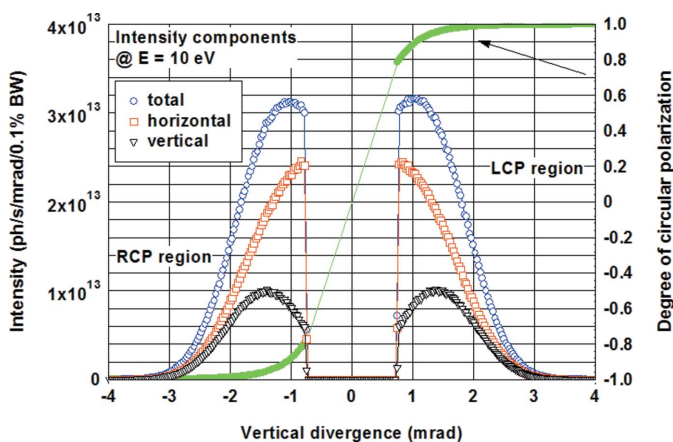


Figure 5 Vertical angular distributions of intensity in total (empty blue circles), horizontal (red squares) and vertical (black triangles) linear polarizations and calculated degree of circular polarization (full green circle) at 10 eV of the beam transmitted by the front-end in the configuration removing aberrations up to and including the coma. The empty area in the center of the figure results from the cold finger placed before the first M1 mirror. LCP: left circularly polarized light. RCP: right circularly polarized light.

250 mm that allows X-rays to pass (see Fig. 7) thus eliminating M1 thermal deformations. This slotted mirror also allows for an additional BM beamline in the soft and hard X-ray domain using the same BM source.

In the case of a current SOLEIL BM source, the beam extraction can be realised using the top-view scheme of Fig. 6, where the BM and quadrupole section are those found at the SMIS (Dumas *et al.*, 2006), AILES (Roy *et al.*, 2006) and DISCO (Giuliani *et al.*, 2009) beamline front-ends. Similarly to SMIS and AILES but in a sideward instead of an upward reflection geometry, the plane mirror M1 is placed in between the BM and the quadrupole chambers at 1 m from the center of source, followed

by the M2 cylindrical mirror. A horizontal extraction of 100 mrad is achievable and the quadrupole chamber next to the BM has to be modified accordingly. Due to the grazing-incidence angles of the M1 and M2 mirrors (22.5°), the beam emerges from M2 perpendicular to the axis of the BM source. The M3 cone-shaped mirror that corrects for the vertical BM aberrations is placed after M2, with a magnification equal to 1 ($p = q = 2.2$ m) in order to remove the vertical coma aberrations. However, due to the lack of space and unlike our previous example, it cannot focus at the same position as the M2 cylindrical mirror. The best cone-shaped profile $R(x) = R_0(1 + ax)$ is obtained from equation (4) for $R_0 = 5.749$ m and $a = 7.30 \times 10^{-4} \text{ mm}^{-1}$ where x is the distance along the axis of curvature of the mirror. Fig. 7 and Table 4 give the main parameters of the VUV beamline front-end in this configuration, with the cylindrical mirror at 1.82 m, where mirror positions are given as optical path distances from the source. The horizontal beamline aperture is 100 mrad and is limited by the length of the first two mirrors. Table 5 gives the beam

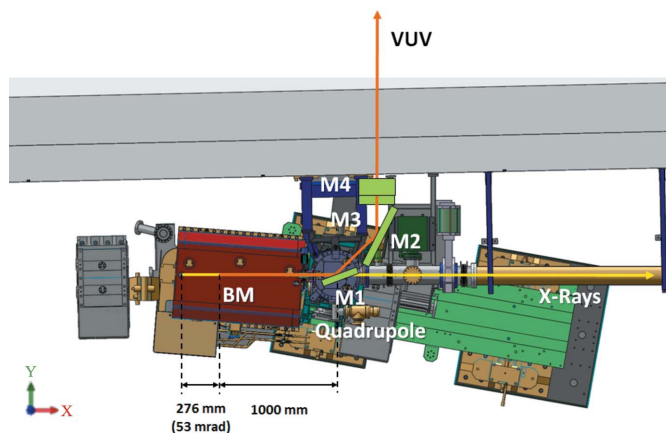


Figure 6 Top view scheme of the BM source and quadrupole arrangement on the SOLEIL front-end. The first two mirrors (M1 plane and M2 cylindrical) are adjacent to the BM source and allow for cancelling the horizontal aberrations up to and including the spherical term.

Table 4
VUV beamline front-end parameters in the configuration where the horizontal BM aberrations including the spherical term are removed.

Element	Optical path distances	Geometry	Footprint @ 99%, $E = 3$ eV, length \times width
Aperture		100 mrad \times 10 mrad (H \times V)	
M1 mirror	1.0 m	Plane, $\theta = 22.5^\circ$, sideward slotted (1.2–1.7 mm aperture)	245 mm \times 10 mm
M2 mirror	1.82 m	Cylinder, horizontal focusing, $\theta = 22.5^\circ$, sideward	440 mm \times 15 mm
M3 mirror	2.2 m	Cone shaped, vertical focusing, $\Delta R/R = \pm 6.6\%$ over ± 90 mm, $\theta = 22.5^\circ$, upward	50 mm \times 155 mm
M4 mirror	2.4 m	Plane, $\theta = 22.5^\circ$, downward	42 mm \times 146 mm
Vertical focusing plane	4.4 m	–	–
Horizontal focusing plane	5.9 m	–	–

Table 5
Optical beam properties at the horizontal and vertical focal planes in the configuration removing the aberrations up to and including the horizontal spherical and up to and including the vertical coma term.

E (eV)	FWHM horizontal size (μm) @ 5.9 m	FWHM vertical size (μm) @ 4.4 m	Divergence (H \times V) (mrad @ 99%)	Flux [photons s^{-1} (0.1% BW) $^{-1}$]
5	349.0	79.7	41.9 \times 7.0	5.8×10^{13}
10	347.6	78.6	41.9 \times 5.7	1.5×10^{14}
20	346.1	78.0	41.9 \times 4.6	1.9×10^{14}

properties (size, divergence, intensity and brilliance) delivered by the front-end for several energies. Fig. 8 shows the beam profiles focused horizontally and vertically at 5.9 m and 4.4 m from the source, respectively. These profiles have Gaussian distributions and indicate that the beam is almost aberration-free. Fig. 9 links the vertical angular distribution of intensity transmitted by the front-end to the energy over the full spectral range (3–20 eV) and the degree of circular polariza-

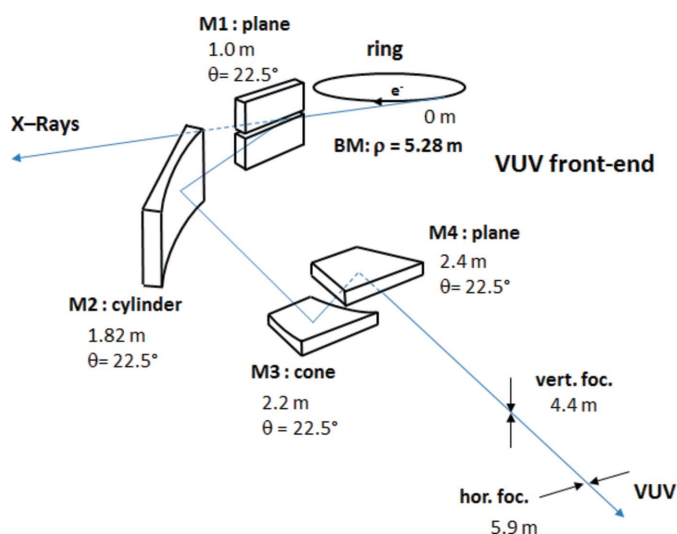


Figure 7
Optical scheme of the SOLEIL VUV beamline front-end in the configuration removing the BM aberrations up to and including the horizontal spherical term and up to and including the vertical coma term. Mirrors positions are given according to the optical path distance from the source.

tion. As in the previous example, the low level of beam aberrations allows having, for CD experiments, well defined vertical transversal areas where the beam is both intense and highly circularly polarized.

The beam emittance at 10 eV of this front-end for a 100 mrad extraction aperture correcting BM source aberrations up to and including the spherical term is $31.5 \text{ mm}^2 \text{ mrad}^2$ (at 99% of the encircled energy), and represents an additional improvement of 30% on the beam emittance per mrad of horizontal aperture compared with that of the previous layout (§3.2) correcting BM source aberrations up to and including the coma term.

4. Conclusion

In this paper, an optical layout removing almost completely the aberrations of BM sources is used in the design of two VUV beamline front-end layouts based on a SOLEIL BM source.

The first design, which uses a common horizontal VUV beamline aperture of 50 mrad, is easily adaptable to the VUV DISCO beamline. Beam properties resulting from both the present DISCO layout and the optimized one are compared, which show that an improvement of over one order of magnitude in the beam emittance can be obtained by cancelling properly the BM source aberrations with the consequent improvement for CD experiments. The second design allows for larger horizontal extractions (100 mrad) by

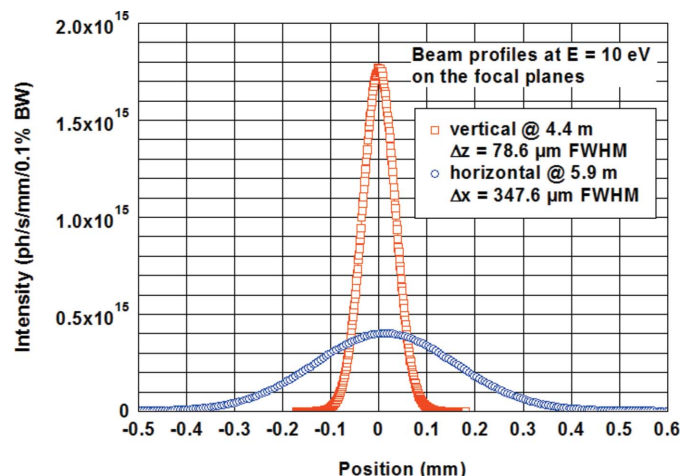


Figure 8
Ray-tracing simulation at 10 eV of the horizontal (blue circles) and vertical (red squares) beam profiles focused at 5.9 m and 4.4 m from the source, respectively, in the configuration removing the horizontal aberrations up to and including the spherical term. The Gaussian shape of the focused beam profiles indicates very low levels of aberrations of the beam delivered by the front-end.

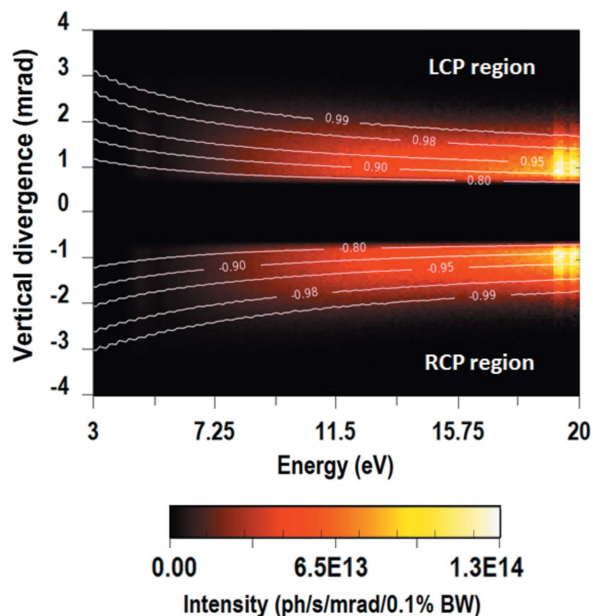


Figure 9 Vertical angular distributions of the intensity transmitted by the front-end as a function of energy and the degree of circular polarization (contour plots) in the configuration removing the horizontal aberrations up to and including the spherical term. The empty area in the center of the image results from the slit in the first M1 mirror that allows hard X-rays to pass through. The low level of beam aberrations allows, for CD experiments, well defined vertical transversal areas where the beam is both intense and highly circularly polarized. LCP: left circularly polarized light. RCP: right circularly polarized light.

placing the first two mirrors of the beamline adjacent to the BM source. This second design, which requires a modification of the present SOLEIL BM and quadrupole chambers, represents an interesting attempt to efficiently integrate magnetic and photonic synchrotron beamline components. These two proposed optical schemes should be considered for future and upgrades to existing VUV beamlines at synchrotron radiation facilities worldwide.

Acknowledgements

The author thanks Paul Dumas for the very active collaboration on IR beamlines which was at the root of the optical

layout used in this paper. The author also thanks Matthieu Réfrégiers, Frédéric Jamme, Alexandre Giuliani, Franck Wien, Valérie Rouam and François Polack for fruitful discussions and advice on the DISCO beamline and the VUV domain. The author also thanks Stéphane Lefrançois for providing SOLEIL BM front-end technical drawings. The author also thanks James Ablett for fruitful discussions on BM SR polarizations.

References

Chubar, O. & Elleaume, P. (1998). *Proceedings of the Sixth European Particle Accelerator Conference (EPAC'98)*, pp. 1177–1179.

Clark Sutherland, J., Desmond, E. & Takacs, P. (1980). *Nucl. Instrum. Methods*, **172**, 195–199.

Dumas, P., Polack, F., Lagarde, B., Chubar, O., Giorgetta, J. L. & Lefrançois, S. (2006). *Infrared Phys. Technol.* **49**, 152–160.

Giuliani, A., Jamme, F., Rouam, V., Wien, F., Giorgetta, J.-L., Lagarde, B., Chubar, O., Bac, S., Yao, I., Rey, S., Herbeaux, C., Marlats, J.-L., Zerbib, D., Polack, F. & Réfrégiers, M. (2009). *J. Synchrotron Rad.* **16**, 835–841.

Hoffmann, A., Kane, A., Nettel, D., Hertzog, D. E., Baumgärtel, P., Lengfeld, J., Reichardt, G., Horsley, D., Seckler, R., Bakajin, O. & Schuler, B. (2007). *Proc. Natl Acad. Sci.* **104**, 105–110.

Howells, M. R. (1992). *Proceedings of the NATO Advanced Study Institute on New Directions in Research with Third-Generation Soft X-ray Synchrotron Radiation Sources*, Maratea, Italy, 28 June–10 July 1992, NATO ASI Series E: Applied Sciences, Vol. 254, p. 359. Dordrecht: Kluwer.

Kimura, S., Kimura, H., Takahashi, T., Fukui, K., Kondo, Y., Yoshimatsu, Y., Moriwaki, T., Nanba, T. & Ishikawa, T. (2001). *Nucl. Instrum. Methods Phys. Res. A*, **467–468**, 437–440.

López-Delgado, R. & Szwarc, H. (1976). *Opt. Commun.* **19**, 286–291.

Moreno, T. (2015). *J. Synchrotron Rad.* **22**, 1163–1169.

Moreno, T. & Idir, M. (2001). *J. Phys. IV Fr.* **11**, 527–531.

Moreno, T., Westfahl, H., Freitas, R. de O., Petroff, Y. & Dumas, P. (2013). *J. Phys. Conf. Ser.* **425**, 142003.

Noda, H., Namioka, T. & Seya, M. (1974). *J. Opt. Soc. Am.* **64**, 1037–1042.

Réfrégiers, M., Wien, F., Ta, H.-P., Premvardhan, L., Bac, S., Jamme, F., Rouam, V., Lagarde, B., Polack, F., Giorgetta, J.-L., Ricaud, J.-P., Bordessoule, M. & Giuliani, A. (2012). *J. Synchrotron Rad.* **19**, 831–835.

Roy, P., Rouzies, M., Qi, Z. M. & Chubar, O. (2006). *Infrared Phys. Technol.* **49**, 139–146.

Zimmerer, G. (2007). *Radiat. Meas.* **42**, 859–864.